Hydrol. Earth Syst. Sci. Discuss., 8, 8671–8700, 2011
www.hydrol-earth-syst-sci-discuss.net/8/8671/2011/
doi:10.5194/hessd-8-8671-2011


Hydrology and Earth System Sciences Discussions



# Reconnoitering the effect of shallow groundwater on land surface temperature and surface energy balance using MODIS and SEBS

**F. Alkhaier[1], Z. Su[1], and G. N. Flerchinger[2]**

[1]Department of water resources, Faculty of Geo-Information Science and Earth Observation, University of Twente, Enschede, The Netherlands
[2]Northwest Watershed Research Center, United States Department of Agriculture, Washington, DC, USA

Received: 7 September 2011 – Accepted: 20 September 2011
– Published: 23 September 2011

Correspondence to: F. Alkhaier (khaier@itc.nl)

Published by Copernicus Publications on behalf of the European Geosciences Union.

## Abstract

The possibility of observing shallow groundwater depth and areal extent using satellite measurements can support groundwater models and vast irrigation systems management. Besides, these measurements help bringing groundwater effect on surface energy balance within land surface models and climate studies. To inspect the MODIS capacity of detecting shallow groundwater effect on land surface temperature and surface energy balance in an area within Al-Balikh River basin in northern Syria, we investigated the interrelationship between in-situ measured water table depths and land surface temperatures of MODIS. Further, we used the Surface Energy Balance System (SEBS) to calculate surface energy fluxes, evaporative fraction and daily evaporation, and inspected their relationships with water table depths. In agreement with the findings of a companion paper (Alkhaier et al., 2011), we found that daytime temperature increased and nighttime temperature decreased with increasing water table depth. Where water table depth increased, net radiation, latent and ground heat fluxes, evaporative fraction and daily evaporation decreased, while sensible heat flux increased. The clear observed relationships resulted from meeting both conditions concluded in the companion paper, i.e. high potential evaporation and big contrast in air temperature. Moreover, the prevailing conditions in this study area helped SEBS producing accurate estimates. We conclude that MODIS is suitable for shallow groundwater effect detection since it has proper imaging times and appropriate sensor accuracy; nevertheless, its coarse spatial resolution is disadvantageous.

## 1 Introduction

Not only do shallow water table conditions characterize low lands in many drainage basins (Freeze and Cherry, 1979), but it has become a general feature in many of the world's large-scale irrigation systems in various countries, i.e. USA, Mexico, China, India, Pakistan, Australia, etc. (Dregne et al., 1996; Rahman, 2008; Umali, 1993;

Middleton and Thomas, 1997; Wichelns, 1999; World Bank, 1992; Xiong et al., 1996). Shallow water table is common in such areas due to high recharge rates, low assimilative capacity of unconfined aquifers and, often, low drainage rates (Northey et al., 2006; Wichelns, 1999).

The possibility of utilizing thermal measurements of operational satellites in observing the depth and the areal extent of shallow groundwater can be of great value in supporting groundwater flow models and in improving the management of vast irrigation systems. Besides, these measurements would be useful in observing the effect of shallow groundwater on surface energy balance, and in bringing that effect within land surface models and climate studies on more solid basis.

To our knowledge, the study by Chase (1969) was one of the earliest attempts to investigate remote sensing capability for mapping the thermal effect of shallow groundwater. In this regard, he found that the (2.5 to 5.6 µm) band was informative and promising.

This early work was followed by the investigation of Myers and Moore (1972) that made use of seasonal flights with thermal radiometers flown over the Sioux Basin in eastern South Dakota. Soil temperature data (8.0 to 14.0 µm) were obtained from predawn missions flown on 7 May, 21 July, 26 August and 12 October 1971. The 26 August imagery showed a broad cool area within the flood plain. This cool area extended over farms with a diversity of land use. Furthermore, a high correlation was found between soil temperature and the aquifer thickness. Their study concluded that late August or early September was the best period for thermal detection of shallow aquifers.

In agreement with the review paper by Becker (2006), and the book by Meijerink et al. (2007), the latest study that we could trace in the literature regarding the investigation of the shallow groundwater effect on land surface temperature was the study of Heilman and Moore (1982). In this study they correlated radiometric temperatures (10.5 to 12.5 µm) from five scenes captured between 5 June and 4 September 1978 by the Heat Capacity Mapping Mission, with water table depths measured on these dates. After empirical correction for vegetation effect, they found that the daytime thermal scene of 4 September had the best correlation. They have demonstrated that radiometric temperature measurements from satellites can be correlated with depth to shallow groundwater if proper deliberations are given to the effect of vegetation. Furthermore they suggested, similar to Huntley (1978), developing a procedure for differentiating groundwater influence from that of soil moisture.

To complete the view, it may worth mentioning here that some remote sensing investigations utilized the thermal effect of shallow water table in influencing snow cover, like delaying and shortening the period of its occurrence over lowlands relative to the surrounding highlands within a watershed (Falconer et al., 1981), or reducing its reflectance and emissivity (Bobba et al., 1992). Where such phenomena occur, visible to near infrared imageries may be more informative than thermal infrared ones.

Despite the humble faculties of earth observation technology during that early period, keen investigations were conducted with regards to tracing shallow groundwater effect on land surface temperature. Nowadays, there are plenty of satellites orbiting the earth and continuously collecting valuable data about the planet surface (Bosilovich et al., 2008). Hence it is quite odd that in spite of the revolutionary development achieved in this technology, there is hardly any study that researched the utilization of this wealth of data in shallow groundwater studies. Furthermore, this data has not been effectively utilized in mapping shallow groundwater effect on land surface temperature and surface energy balance components thus far.

In a companion paper (Alkhaier et al., 2011) we presented a detailed description of how shallow groundwater affects surface soil moisture, surface soil temperature and the various components of surface energy balance. We also discussed the optimum conditions under which this effect can be sufficiently clear to be detected using satellite measurements.

In this paper we aimed at inspecting the capacity of MODIS (Moderate-resolution Imaging Spectroradiometer) to detect the effect of shallow groundwater on surface temperature of an area within Al-Balikh River basin in northern Syria, using day and night images. Also we aimed at reconnoitering the spatial distribution of shallow groundwater effect on surface energy balance components, soil moisture, evaporative fraction and daily evaporation in this area at the day of image acquisition.

In this study, we investigated the interrelationship between water table depths measured in the field and land surface temperatures retrieved from two MODIS images (day and night) shot within the timeframe of our field campaign. Also we used the Surface Energy Balance System (SEBS) to calculate the maps of surface energy balance, evaporative fraction and daily evaporation. The spatial relationships of water table depth with these parameters were then inspected and analyzed. Hereinafter we give a brief description of collecting and handling both field measurements and remote sensing data.

## 2 Study area description and data collection

### 2.1 Field data

During a short period (13 to 17 January 2007) we conducted a field campaign within Al-Balikh river basin in northern Syria supported by the General Organization for Land Reclamation, Ar-Raqqa. The campaign covered an area of about 186 $km^2$, between latitude 36°02′ to 36°13′ N and longitude 38°46′ to 39°03′ E (Fig. 1).

The study area represents a flat region of reclaimed agricultural fields. Hence, there is no considerable topographic relief within the area under consideration. The Digital Elevation Model retrieved from the ASTER Global Digital Elevation Model (GDEM, 30 m pixel resolution) shows that the flat study area level ranges between approximately 265 m and 285 m a.m.s.l. (Fig. 2a).

At the campaign time, the majority of the fields in the study area were fallow. Yet, few spots were planted by winter wheat and vegetables. Figure 2b shows the Normalized Difference Vegetation Index (NDVI) map at 17 January, which was calculated using the MODIS red and near-infrared bands (250 m pixel resolution), centered at 645 nm and



HESSD
8, 8671–8700, 2011

858 nm respectively. The NDVI values within the study domain were low demonstrating the predominance of bare soil conditions.

Somewhat poorly drained soils are predominant in this area, and in many places, shallow water tables exists all year round. Water table depth in the area ranges between 1 and 10 m. Generally, soils of the surface layer can be classified as silty clay; furthermore clayey horizons may be encountered at different shallow depths throughout the basin.

The area is characterized by steppe climate (Köppen climate classification), which is a semi-dry climate with an average annual rainfall of less than 200 mm. The weather data used in this study were obtained from the nearby weather station (Ar-Raqqa, 35°57′ N, 39°00′ E). The field campaign days were mostly sunny. The prevalent wind was dry cold northerly wind with an average speed of 2.6 $ms^{-1}$. In this area, air temperature usually has a high contrast between day and night. During the field campaign period, air temperatures fell to −5 °C in nighttime and rose to 14 °C in daytime.

Somewhere between mid November and mid February, the main irrigation canal that supplies the whole area is usually blocked in favor of maintenance for about one and half months. A month before our field campaign the irrigation activity had been stopped. By that we were assured that there were no intense water table fluctuations in the period of our measurements.

Data of water table depth and surface soil moisture was collected from about 90 locations. Soil moisture of the upper 5 cm was measured in-situ using Stevens' Hydra probe. Additionally, some soil samples were brought to the laboratory for texture analysis and soil moisture verification. Water table depth which was measured manually using a simple sounding device ranged between 1m and 8 m. Raster maps of soil moisture and water table depth were generated starting from the point data by means of a moving average interpolation.





HESSD
8, 8671–8700, 2011

## 2.2 Remote sensing data

Being rich in spectral bands with moderate spatial resolution, and providing free-of-charge images at four different times per day, MODIS instrument was chosen to be exploited in our research. The scientific instrument is operating on board two currently operational spacecrafts (Terra and Aqua), and captures images of 36 spectral bands ranging in wavelength between 0.4 µm and 14.4 µm. The numerous bands of MODIS have three spatial resolutions: 250 m, 500 m, and 1000 m, and provide valuable data regarding land cover type and dynamics, vegetation indices, land surface temperature, emissivity and albedo.

Two MODIS level 1B images of 17 January 2007 were the clearest within the field work timeframe; hence they were used in this study. Using MODIS Reprojection Swath Tool (MRTSwath), each radiances-calibrated level 1B image was transformed from HDF-EOS swath format to a UTM projected GeoTIFF image and resampled for 1km pixel size. Next, it was imported to the Integrated Land and Water Information System (ILWIS) for further processing and surface energy balance calculations. This included: raw data to radiance or reflectance transformation; brightness temperature computation and atmospheric correction. Within the framework of SEBS, we calculated land surface albedo, emissivity, temperature, vegetation indexes, surface energy fluxes, evaporative fraction and actual daily evaporation.

# 3 Surface energy balance and related maps calculations

SEBS is an advanced remote sensing algorithm developed by Su (2001) for the estimation of atmospheric turbulent fluxes maps using satellite data. It has been extensively applied and validated with a variety of methods in different regions and climates (Su, 2002; Jia et al., 2003, 2009; Su et al., 2005; McCabe and Wood, 2006; McCabe et al., 2008; Pan et al., 2008; Badola, 2009; van der Kwast et al., 2009; Gibson et al., 2011).





HESSD
8, 8671–8700, 2011

Calculating surface energy fluxes by means of SEBS involves using two types of data: spatially distributed variables (maps) and in-situ measured variables. The first type can be derived from remote sensing data and includes land surface albedo, emissivity, temperature, vegetation indexes and roughness height. The second type can be obtained from local weather stations and includes air pressure, temperature, humidity, wind speed and solar radiation.

SEBS algorithm is composed of: a set of equations to obtain land surface albedo, emissivity, temperature, vegetation indexes from satellite data; an extended model for calculating the roughness length for heat transfer; and a formulation for obtaining sensible heat flux by an iterative process. After estimating all four terms of the surface energy balance (Eq. 1) using SEBS, additional important physical information can be retrieved easily, such as evaporative fraction, daily evaporation and surface soil moisture.

$$R_\mathrm{n} = G + H + \mathrm{LE}. \tag{1}$$

Net radiation, $R_\mathrm{n}$, is calculated as the outcome of radiation at land surface:

$$R_\mathrm{n} = (1 - \alpha)\, K_\mathrm{in} + \varepsilon\, L_\mathrm{in} - \varepsilon\sigma\, T_\mathrm{s}^4 \tag{2}$$

where $K_\mathrm{in}$ and $L_\mathrm{in}$ are the incoming shortwave and longwave radiations respectively, $\alpha$, $\varepsilon$ and $T_\mathrm{s}$ are land surface albedo, emissivity and temperature respectively, and $\sigma$ is Stefan-Boltzmann constant.

Ground heat flux, $G$, is simply calculated as a ratio of net radiation, $R_\mathrm{n}$, depending on the fractional canopy coverage $f_\mathrm{c}$ of the studied area:

$$G = R_\mathrm{n} \left[0.05 + 0.265\,(1 - f_\mathrm{c})\right]. \tag{3}$$

Sensible heat flux, $H$, is calculated using Monin–Obukhov similarity (MOS) theory. Within the Atmospheric Surface Layer (ASL), the bottom (10 %) of the Atmospheric Boundary Layer (ABL) and above the roughness sub-layer, the similarity relationships for wind speed and temperature profiles can be expressed as:





HESSD
8, 8671–8700, 2011

$$u = \frac{u_*}{k}\left[\ln\left(\frac{z - d_0}{z_{z_{om}}}\right) - \Psi_m\left(\frac{z - d_0}{Ol}\right) + \Psi_m\left(\frac{z_{om}}{Ol}\right)\right] \tag{4}$$

$$\theta_s - \theta_a = \frac{H}{k\, u_*\, \rho_a\, c_a}\left[\ln\left(\frac{z - d_0}{z_{z_{oh}}}\right) - \Psi_h\left(\frac{z - d_0}{Ol}\right) + \Psi_h\left(\frac{z_{oh}}{Ol}\right)\right]. \tag{5}$$

In which $u$ is the average wind speed, $\theta_s$ and $\theta_a$ are the potential temperatures at land surface and at the reference height $z$ respectively, $u_*$ is wind friction velocity, $k$ is von Karman's constant, $d_0$ is the zero plane displacement height, $z_{om}$ and $z_{oh}$ are the roughness heights for momentum and heat transfer respectively, $\Psi_m$ and $\Psi_h$ are stability correction functions for momentum and heat transfer respectively, $\rho_a$ and $c_a$ are air density and specific heat correspondingly and Ol is the Obukhov length which is expressed as:

$$Ol = \frac{\rho_a\, c_a\, u_*^3\, \theta_v}{k\, g\, H} \tag{6}$$

where $\theta_v$ is the virtual potential temperature near land surface and $g$ is the gravitational acceleration.

Sensible heat flux, $H$, and latent heat flux, LE, are derived from Eqs. (4) to (6) using an iterative process and controlled by two bounding limits (i.e. wet and dry conditions). Within the course of this iterative process, the relative evaporation, $\Lambda_r$, which is the ratio between the actual and the potential latent heat fluxes, LE and $LE_{wet}$, is calculated by:

$$\Lambda_r = \frac{LE}{LE_{wet}} = 1 - \frac{H - H_{wet}}{H_{dry} - H_{wet}} \tag{7}$$

where $H_{wet}$ and $H_{dry}$ are the sensible heat fluxes at the wet and the dry limits respectively. For further details the reader is referred to Su (2002, 2005).





HESSD
8, 8671–8700, 2011

The evaporative fraction, $\Lambda$, which is the ratio between the energy consumed for actual evapotranspiration and the net available energy can be calculated from:

$$\Lambda = \frac{\text{LE}}{R_n - G} = \frac{\text{LE}}{\text{LE} + H}. \quad (8)$$

Finally, the actual daily evaporation can be estimated as:

$$E_{\text{daily}} = 8.64 \times 10^7 \times \overline{\Lambda} \times \frac{\overline{R_n} - \overline{G}}{L \, \rho_w}. \quad (9)$$

According to Su (2005), the evaporative fraction, $\overline{\Lambda}$, is conservative and can be approximated by the SEBS estimate, i.e. $\Lambda$. $\overline{R_n}$ and $\overline{G}$ are the daily values of net radiation and soil heat flux respectively, $L$ is the latent heat of vaporization and $\rho_w$ is water density. The daily upshot of soil heat flux is small and can be neglected, and the daily net radiation, $\overline{R_n}$, is calculated by:

$$\overline{R_n} = (1 - \alpha)\,\overline{K_{in}} + \varepsilon\,\overline{L} \quad (10)$$

where $\overline{K_{in}}$ is the daily incoming radiation and $\overline{L}$ is daily net longwave radiation.

The evaporative fraction proved to be a suitable indicator of soil moisture conditions. Using datasets from USA and Spain, Bastiaanssen et al. (2000) demonstrated that volumetric soil moisture can be estimated using a statistical relationship between evaporative fraction and soil moisture of the vadose zone. This relationship was later modified by Scott et al. (2003) to involve the degree of saturation ($\theta/\theta_{sat}$):

$$\frac{\theta}{\theta_{sat}} = \exp\left\{(\Lambda - 1)/0.42\right\} \quad (11)$$

where $\theta$ and $\theta_{sat}$ are the actual and the saturated volumetric soil moisture respectively. By validating the accuracy of this relationship with data from irrigated plains in Pakistan and Mexico, Scott et al. (2003) demonstrated that it is a kind of a standard relationship which can be applied to a wide range of soils.





HESSD
8, 8671–8700, 2011

To inspect the spatial relationships between groundwater depth map and the variant parameters' maps we carried out the Cross operation in ILWIS between the relevant raster maps. The Cross operation performs an overlay of two raster maps by comparing pixels at the same positions in both maps and outputs all the combinations that occur between the values in both maps in an output cross-table. Afterwards, the results in each cross-table were plotted accordingly.

## 4 Results and discussion

### 4.1 Water table depth and soil moisture maps

The two raster maps showing the spatial distributions of water table depth and soil moisture were interpolated from the point data collected in the field (Fig. 3). Areas in the vicinity to Al-Balikh River (the eastern area) and in Wadi Al-Faied (the south western area) have deeper water table (Fig. 3a) and lower level of soil moisture (Fig. 3b), while the remaining area has shallower water table and higher level of soil moisture.

The deeper water table conditions in Al-Balikh River and Wadi Al-Faied are most likely attributable to the relatively better drainage conditions. A historical False Color Composite (FCC) image captured by the Multispectral Scanner System (MSS) sensor on board of Landsat2 on 8 August 1975 (Fig. 4), demonstrates that the areas with deeper water table correspond to very old cultivated land. On the other hand, the newly cultivated area had shallower water table demonstrating poorer drainage conditions.

The cross-relationship between water table depth and surface soil moisture is plotted in Fig. 5, and explains that soil moisture clearly increased starting from a water depth of 4 m and up. Where the water table was deeper than 4 m, surface soil moisture seems not to be affected by water table level.





HESSD
8, 8671–8700, 2011

## 4.2 Soil temperature maps

By inspecting both day and night maps of land surface temperature extracted from the two MODIS images of 17 January, we find that areas of deeper water table depth were warmer at daytime and cooler in nighttime (Fig. 6).

Plotting the cross-relationships (Fig. 7) between water table depth and day and night temperatures at 17 January 2007 showed that, down to 4 m water depth, daytime temperature increased (Fig. 7a) and nighttime temperature decreased with increasing water table depth (Fig. 7b).

## 4.3 Surface energy balance maps

The instantaneous maps of surface energy balance at 10:25 LT calculated via SEBS are shown in Fig. 8. There was a clear trend in the variant energy fluxes to follow the spatial distribution of the water table depth shown in Fig. 3a. The areas with shallower water table had higher latent heat flux but lower sensible heat flux in comparison to the areas with deeper water table depth (Fig. 8b and c). The trend was less sharp for the net radiation and ground heat flux (Fig. 8a and d). Yet, shallow groundwater areas tended to have higher positive net radiation and ground heat flux. The cross-relationships plotted in Fig. 8 show that both latent and sensible heat fluxes had sharper trend to follow water table depth than net radiation and ground heat flux had. In agreement with the findings and results of the companion paper (Alkhaier et al., 2011), net radiation, latent and ground heat fluxes, decreased with increasing water table depth, while sensible heat flux increased with increasing water table depth.

We notice that some pixels within the shallower groundwater areas had lower values than the general trend regarding net radiation and ground heat flux (Fig. 9a and d). Investigating the reason behind this phenomenon revealed that some spots of these areas suffer soil salinity (Alkhaier, 2003). Where salt crust accumulates at land surface, it increases the albedo (Fujimaki et al., 2003); this in turn magnifies the reflected shortwave radiation (Eq. 2) and diminishes net radiation. Since ground heat flux is





HESSD
8, 8671–8700, 2011

calculated in SEBS as a ratio of net radiation (Eq. 3), it is diminished also at these pixels (Fig. 9d).

### 4.4 The evaporative fraction and the actual daily evaporation

Figure 10 shows the cross-relationships between water table depth and both the evaporative fraction and the actual daily evaporation. Both parameters had their highest values for shallower water table depth. They become smaller with increasing water table depth. Comparing the values of the daily evaporation with the measured pan evaporation (Class A) from the nearby weather station (2.4 mm) for this day (17 January) certifies that the SEBS estimates of the energy fluxes were reasonable.

### 4.5 The soil moisture map estimated from SEBS' actual daily evaporation

Both maps of soil moisture measured in the field and soil moisture estimated from SEBS evaporative fraction were plotted against each other in Fig. 11, in which we find very good agreement ($R^2 = 0.7506$). Yet, the calculated soil moisture was slightly underestimated for lower levels of soil moisture and a little overestimated for higher levels of soil moisture. We ascribe this phenomenon to the fact that Eq. (11) was originally developed for soil moisture of the complete vadose zone (Bastiaanssen et al., 2000; Scott et al., 2003) whereas the measured soil moisture was only for the upper 5 cm. The agreement between the two soil moisture maps affirms the reasonability of SEBS calculations.

## 5 Conclusions and recommendations

We conclude that it is possible to map the effect of shallow groundwater on land surface temperature using the freely available satellite data like MODIS. Satellite measurements demonstrated a clear correspondence of surface temperature with water table depth both during daytime and night. In parallel, our field measurements demonstrated a clear relationship between surface soil moisture and water table depth. Consequently, the various surface energy balance maps, calculated using SEBS and MODIS data, correlated well with water table depth. Finally it was possible using the SEBS estimate of evaporative fraction to estimate soil moisture distribution in the area reasonably.

Many factors played a substantial role in the good results of our investigation. In view of the conclusions of the companion paper (Alkhaier et al., 2011) with regards to the favorable conditions for detecting the effect of shallow groundwater via thermal remote sensing, we find that the two major conditions were met in this day. Whereas the effect of latent heat flux was clear at daytime due to the relatively high potential evaporation under the prevalent dry and sunny conditions, the effect of volumetric heat capacity was clear owing to the high contrast in air temperature between day and night. In this way the circumstances were most expedient for water table depth detection using thermal remote sensing.

The suspension of irrigation activity together with the scantiness of rain incidents for quite some time before the measurement campaign made surface soil moisture and water table depth conditions fairly stable. We may add here that the short period of our measurement campaign facilitated obtaining reliable data of the two state variables (i.e. soil moisture and water table depth).

Having limited vegetation cover in the study area was advantageous regarding avoiding possible perturbations and complexities imposed by plants on surface temperature measurements. Further investigations of such circumstances, using remote sensing data supported by numerical simulations, are recommended. Actually, the authors are working on this issue.

The limited topographic relief and vegetation cover in the study area helped to avoid possible uncertainty sources (Gibson et al., 2011) in SEBS estimates of energy fluxes. The correspondence of the derived daily evaporation and soil moisture with in field measured values proved that the utilization of SEBS in this area was a success.





HESSD
8, 8671–8700, 2011

The exploitation of MODIS in this study proved to be an excellent choice, since it has many convenient characteristics. The imaging times were appropriate to detect the thermal effect of groundwater at both day and night. Shooting the area four times per day secured abundance in imageries, which in turn improved the chance of finding clear and reliable scenes. Next to the commonly used spectral bands of MODIS for obtaining valuable information about the study area (i.e. vegetation indices, albedo, emissivity, temperature, etc.), we found that bands 20 and 22, centered at 3.75 µm and 3.959 µm respectively, were specifically useful to ascertain that the image is free from perturbation by thin clouds. Concerning sensor accuracy, precision and resolution, MODIS demonstrated satisfactory efficacy. Even at nighttime when land surface temperature ranged within only two degrees Celsius, MODIS could delineate the groundwater effect suitably.

The only feature that prevented MODIS from being perfect for the purpose of our study is the spatial resolution of its thermal bands, i.e. bands 31 and 32 centered at 11.03 µm and 12.02 µm respectively. The 1000 m pixel of the thermal bands may contain the effect of unrelated surfaces (i.e. vegetated or residential areas, roads, canals, etc.). This was a main reason behind the outliers in the cross-relationship figures. Possible finer resolution in future satellites may enable masking out the undesired effect of such unrelated surfaces, and make the thermal mapping of shallow aquifers more precise.

All cross-relationship figures illustrate that the depth of approximately 4m is the critical depth above which groundwater affects surface soil moisture and temperature, and consequently all the surface energy balance components. This critical depth may be a peculiarity for this area and may differ from one region to another according to the conditions of the predominant soils.

The thermal mapping of shallow groundwater demonstrated in this study may be involved in transient three-dimensional groundwater models, especially when these models consider the dynamic interrelationship between the aquifer and the soil moisture above water table. In addition, mapping shallow groundwater effect on surface energy fluxes using remote sensing will be of great help in assessing the interactions among groundwater dynamics, land surface processes and the atmosphere.

Finally, some researches suggested developing a procedure for extricating groundwater influence from that of soil moisture (Heilman and Moore, 1982; Huntley, 1978). We believe that this procedure is not necessary provided that remote sensing investigations are accompanied with appropriate relevant numerical simulations. In fact, the results of this paper together with those of the companion paper (Alkhaier et al., 2011) illustrate clearly that the two profiles respond differently to rain incidents in a way that they still differ in surface soil moisture.

*Acknowledgements.* The authors are grateful to the staff of General Organization for Land Reclamation, Ar-Raqqa, Syria, for supporting our field campaign. We specifically mention Geologist Tareef Al-Naeif, and Geologist Hassan Al-Eeisa. The MODIS data used in this research are distributed by the Land Processes Distributed Active Archive Center (LP DAAC), located at the US Geological Survey (USGS) Earth Resources Observation and Science (EROS) Center (lpdaac.usgs.gov). The authors highly appreciate the editor Harrie-Jan Hendricks Franssen, and the reviewers for their sincere efforts and constructive comments.

## References

Alkhaier, F.: Soil Salinity Detection Using Satellite Remote Sensing, M.Sc. thesis, International Institute for Geo-Information Science and Earth Observation, The Netherlands, 2003.

Alkhaier, F., Flerchinger, G. N., and Su, Z.: The effect of shallow groundwater on land surface temperature and surface energy balance under the conditions of bare soil: modeling and description, Hydrol. Earth Syst. Sci. Discuss., 8, doi:10.5194/hessd-8-8639-2011, 8639–8670, 2011.

Badola, A.: Validation of Surface Energy Balance System (SEBS) over Forest Land Cover and Sensitivity Analysis of the Model, M.Sc. thesis, International Institute for Geo-information Science and Earth Observation, The Netherlands, 2009.

Bastiaanssen, W. G. M., Molden, D. J., and Makin, I. W.: Remote sensing for irrigated agriculture: examples from research and possible applications, Agr. Water Manage., 46, 137–155, 2000.





HESSD

8, 8671–8700, 2011

Reconnoitering the effect of shallow groundwater on land surface temperature

F. Alkhaier et al.

Becker, M. W.: Potential for satellite remote sensing of ground water, Ground Water, 44, 306–318, 2006.
Bobba, A. G., Bukata, R. P., and Jerome, J. H.: Digitally processed satellite data as a tool in detecting potential groundwater flow systems, J. Hydrol., 131, 25–62, 1992.
Bosilovich, M., Hook, S., Knuteson, R., Pinheiro, A., Prigent, C., Rossow, W., and Viterbo, P.: International Workshop on the Retrieval and Use of Land Surface Temperature: Bridging the Gaps, Summary Report, NOAA's National Climatic Data Center (NCDC), Asheville, 7–9 April 2008.
Chase, M. E.: Airborne remote sensing for groundwater studies in prairie environment, Can. J. Earth Sci., 6, 737–741, 1969.
Dregne, H. E., Xiong, Z., and Xiong, S.: Soil salinity in China, Desertification Control Bull., 28, 28–33, 1996.
Falconer, A., Myers, L., and Deutsch, M.: Observations on Lake Ontario Basin hydrology from optical enhancements of Landsat imagery, in: Satellite Hydrology, edited by: Deutsch, M., Weisnet, D. R., and Rango, A., American Water Resources Association, Minneapolis, Minnesota, 427–436, 1981.
Freeze, R. A. and Cherry, J. A.: Groundwater, Prentice-Hall, Inc. Englewood Cliffs, NJ, 1979.
Fujimaki, H., Shiozawa, S., and Inoue, M.: Effect of salty crust on soil albedo, Agr. Forest Meteorol., 118, 125–135, doi:10.1016/S0168-1923(03)00110-2, 2003.
Gibson, L. A., Münch, Z., and Engelbrecht, J.: Particular uncertainties encountered in using a pre-packaged SEBS model to derive evapotranspiration in a heterogeneous study area in South Africa, Hydrol. Earth Syst. Sci., 15, 295–310, doi:10.5194/hess-15-295-2011, 2011.
Heilman, J. L.,and Moore, D. G.: Evaluating depth to shallow groundwater using heat capacity mapping mission (HCMM) data, Photogramm. Eng. Rem. S., 48, 1903–1906, 1982.
Huntley, D.: On the detection of shallow aquifers using thermal infrared imagery, Water Resour. Res., 14, 1075–1083, 1978.
Jia, L., Su, Z., van den Hurk, B., Menenti, M., Moene, A., de Bruin, H. A. R., Yrisarry, J. J. B., Ibanez, M., and Cuesta, A.: Estimation of sensible heat flux using the Surface Energy Balance System (SEBS) and ATSR measurements, Phys. Chem. Earth, 28, 75–88, 2003.
Jia, L., Xi, G., Liu, S., Huang, C., Yan, Y., and Liu, G.: Regional estimation of daily to annual regional evapotranspiration with MODIS data in the Yellow River Delta wetland, Hydrol. Earth Syst. Sci., 13, 1775–1787, doi:10.5194/hess-13-1775-2009, 2009.

McCabe, M. F. and Wood, E. F.: Scale influences on the remote estimation of evapotranspiration using multiple satellite sensors, Remote Sens. Environ., 105, 271–285, 2006.
McCabe, M. F., Wood, E. F., Wojcik, R., Pan, M., Sheffield, J., Gao, H., and Su, H.: Hydrological consistency using multi-sensors remote sensing data for water and energy cycle studies, Remote Sens. Environ., 112, 430–444, 2008.
Meijerink, A. M. J., Bannert, D., Batelaan, O., Lubczynski, M. W., and Pointet T.: Remote Sensing Applications to Groundwater, Paris, United Nations Educational Scientific and Cultural Organization (UNESCO), 2007.
Middleton, N., and Thomas, D.: World Atlas of Desertification, 2, Wiley, publisher Arnold United Nations Environment Programme (UNEP), New York, 1997.
Myers, V. I. and Moore, D. G.: Remote sensing for defining aquifers in glacial drift, Eighth International Symposium on Remote Sensing of Environment, 1, University of Michigan, 715–728, 1972.
Northey, J. E., Christen, E. W., Ayars, J. E., and Jankowski, J.: Occurrence and measurement of salinity stratification in shallow groundwater in the Murrumbidgee Irrigation Area, south-eastern Australia, Agr. Water Manage., 81, 23–40, 2006.
Pan, M., Wood, E. F., Wojcik, R., and McCabe, M. F.: Estimation of regional terrestrial water cycle using multi-sensor remote sensing observations and data assimilation, Remote Sens. Environ., 112, 1282–1294, 2008.
Rahman, A.: A GIS based DRASTIC model for assessing groundwater vulnerability in shallow aquifer in Aligarh, India, Appl. Geogr., 28, 32–53, 2008.
Scott, C. A., Bastiaanssen, W. G. M., and Ahmad, M. D.: Mapping spatio-temporal distributions of soil moisture throughout irrigated watersheds using optical and high resolution imagery, J. Irrig. Drain. Eng.-ASCE, 129, 326–335, 2003.
Su, H., McCabe, M. F., and Wood, E. F.: Modeling evapotranspiration during SMACEX: Comparing two approaches for local and regional-scale prediction, J. Hydrometeorol. – Special Section, 6, 910–922, 2005.
Su, Z.: A Surface Energy Balance System (SEBS) for estimation of turbulent heat fluxes from point to continental scale, Publications of the National Remote Sensing Board (BCRS), USP-2, 2001.
Su, Z.: The Surface Energy Balance System (SEBS) for estimation of turbulent heat fluxes, Hydrol. Earth Syst. Sci., 6, 85–100, doi:10.5194/hess-6-85-2002, 2002.

Su, Z.: Estimation of the surface energy balance, in: Encyclopedia of Hydrological Sciences, edited by: Anderson, M. G. and McDonnell, J. J., 2, Wiley and Sons, 731–752, 2005.
Umali, D. L.: Irrigation–Induced Salinity: A Growing Problem for Development and the Environment, Technical Paper 215, World Bank, Washington, DC, 1993.
van der Kwast, J., Timmermans, W., Gieske, A., Su, Z., Olioso, A., Jia, L., Elbers, J., Karssenberg, D., and de Jong, S.: Evaluation of the Surface Energy Balance System (SEBS) applied to ASTER imagery with flux-measurements at the SPARC 2004 site (Barrax, Spain), Hydrol. Earth Syst. Sci., 13, 1337–1347, doi:10.5194/hess-13-1337-2009, 2009.
Wichelns, D.: An economic model of waterlogging and salinization in arid regions, Ecol. Econ., 30, 475–491, 1999.
World Bank: Development and the Environment, World Development Report, World Bank, Washington, DC, 1992.
Xiong, S., Xiong, Z., and Wang, P.: Soil salinity in the irrigated area of the Yellow River in Ningxia, China, Arid Soil Res. Rehab., 10, 95–101, 1996.

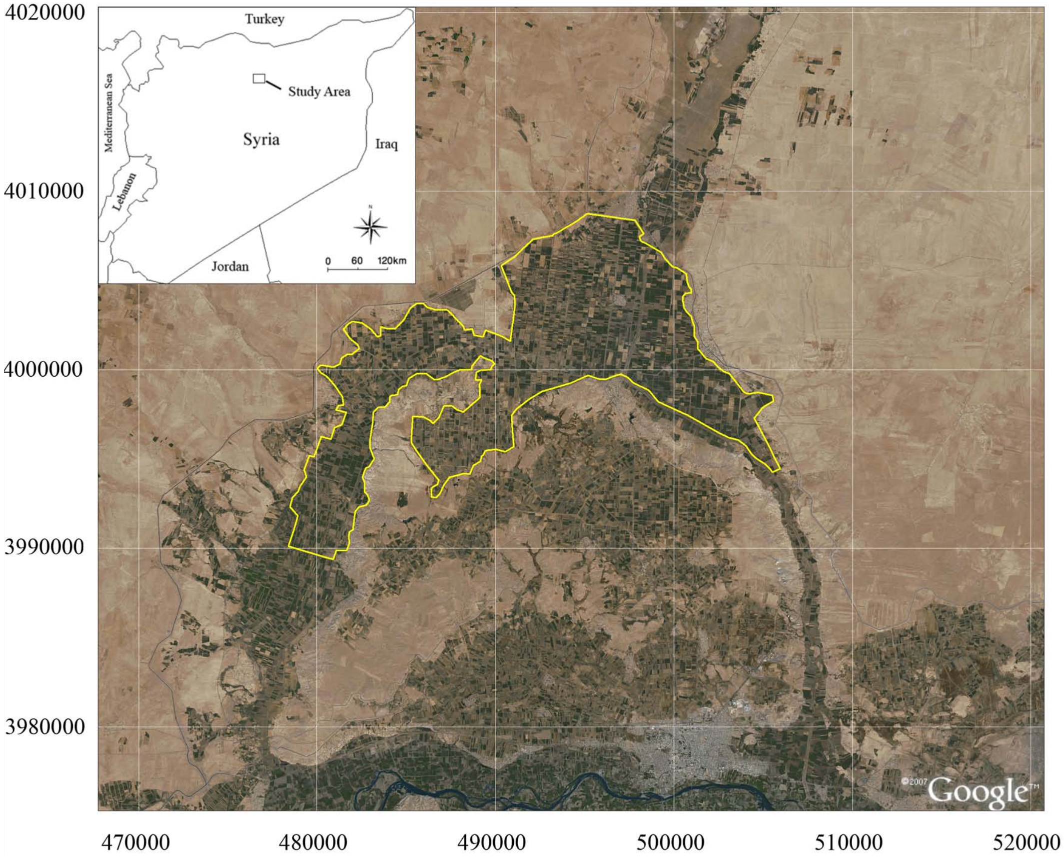


**Fig. 1.** Study area location within Al-Balikh river basin in northern of Syria (Google Earth image).

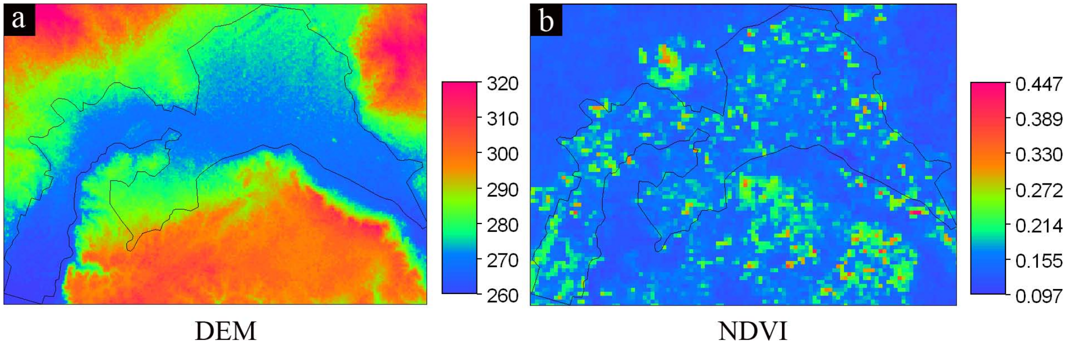


**Fig. 2.** **(a)** Digital Elevation Model (30 m pixel resolution), and **(b)** NDVI map of the study area (250 m pixel resolution).





HESSD
8, 8671–8700, 2011

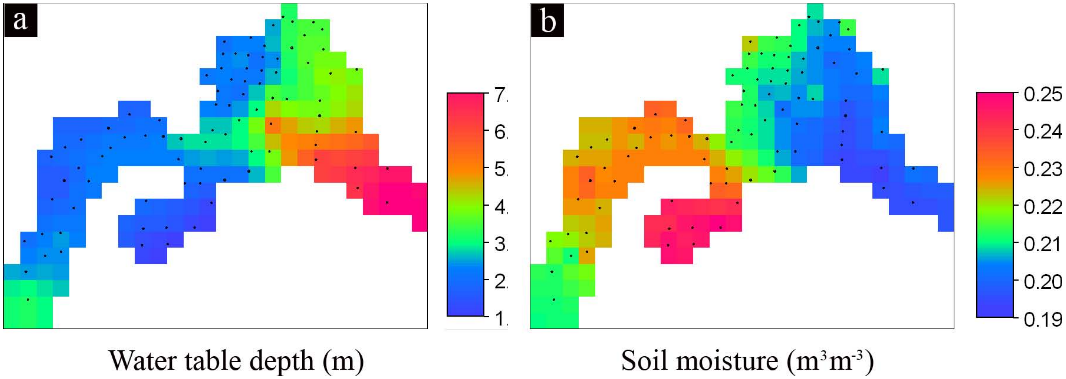


**Fig. 3.** The interpolated raster maps for **(a)** water table depth and **(b)** soil moisture of the upper 5 cm. Locations of the point data collected in the field are also shown.

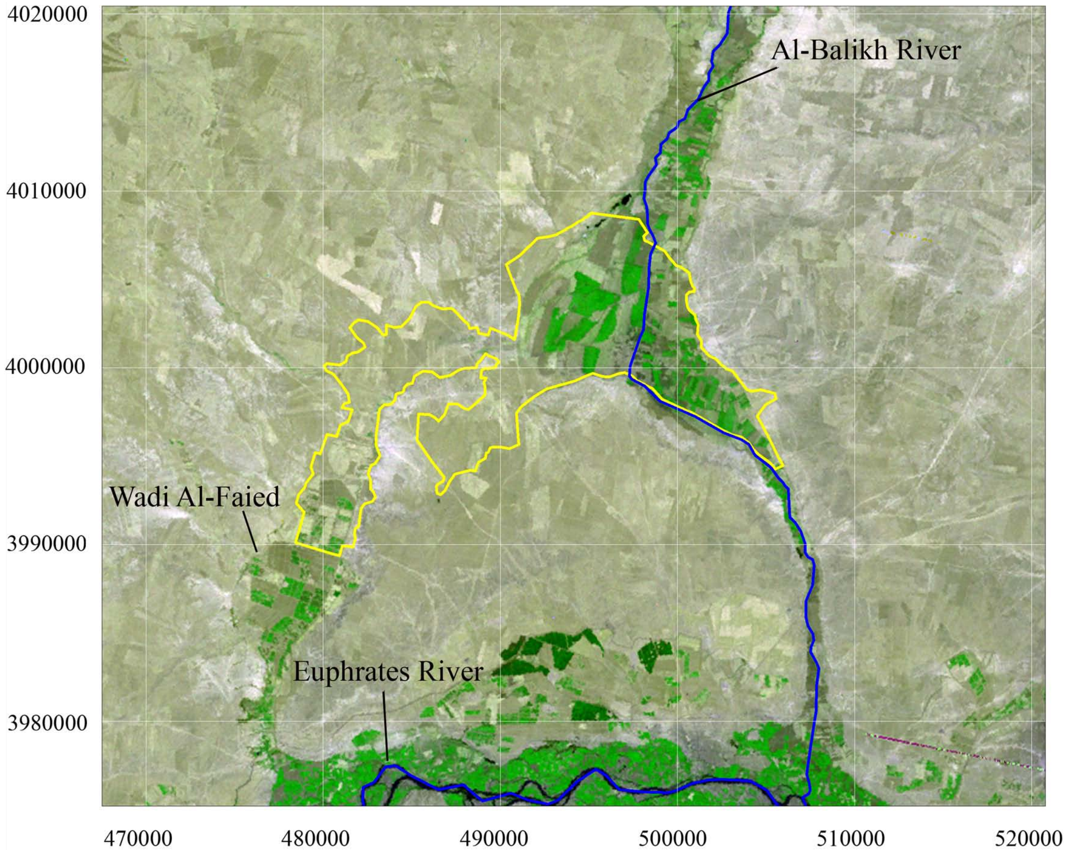


**Fig. 4.** Landsat2, False Color Composite (Red = band 5; Green = band 6; Blue = band 4), 8 August 1975, 09:34 LT.

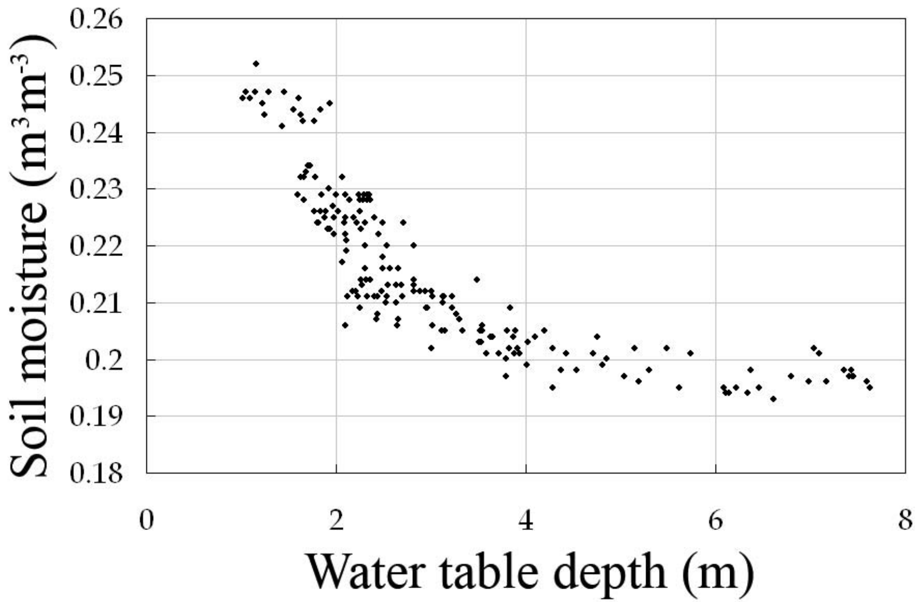


**Fig. 5.** The cross-relationship between water table depth map and surface soil moisture map.





HESSD
8, 8671–8700, 2011

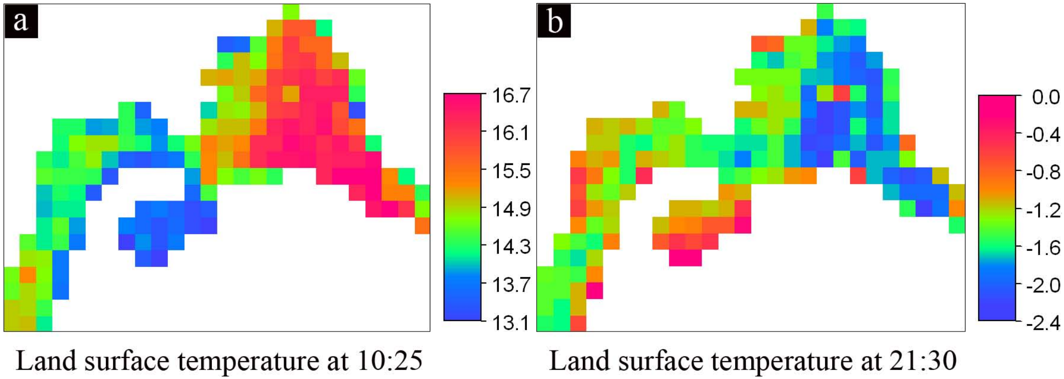


**Fig. 6.** Land surface temperature maps (°C) of the study area on 17 January 2007. **(a)** Daytime temperature, and **(b)** nighttime temperature.





HESSD
8, 8671–8700, 2011

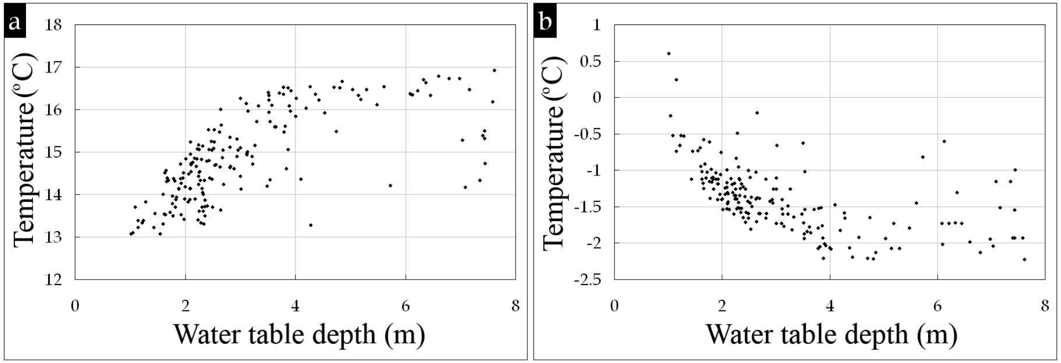


**Fig. 7.** Cross-relationships between water table depth and **(a)** daytime land surface temperatures and **(b)** nighttime land surface temperatures at 17 January 2007.





HESSD
8, 8671–8700, 2011

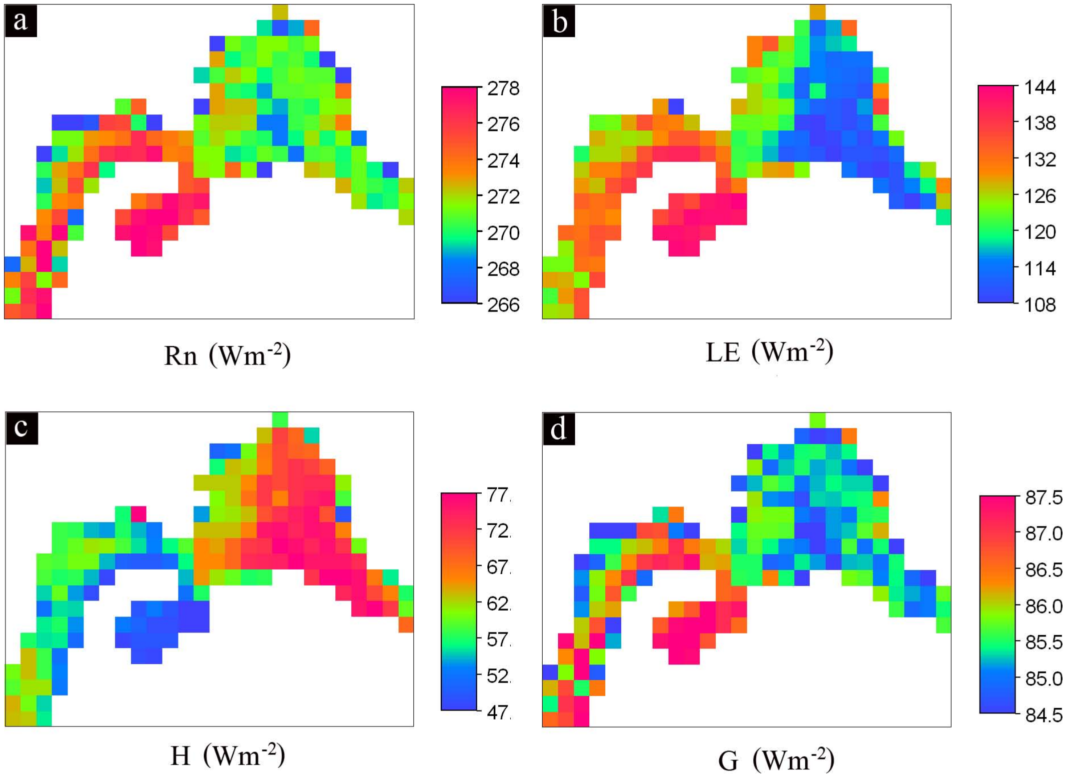


**Fig. 8.** The SEBS calculated maps of the instantaneous components of surface energy balance on 17 January 2007, 10:25 LT.





HESSD
8, 8671–8700, 2011

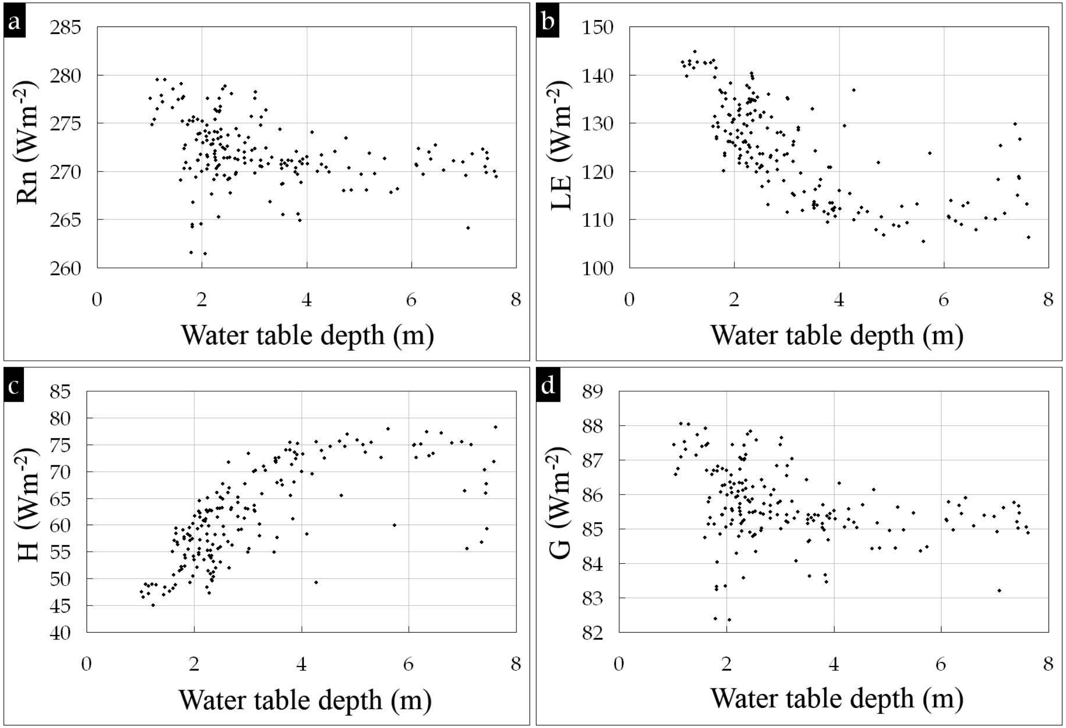


**Fig. 9.** The cross-relationships between water table depth and the variant instantaneous components of surface energy balance on 17 January 2007, 10:25 LT.

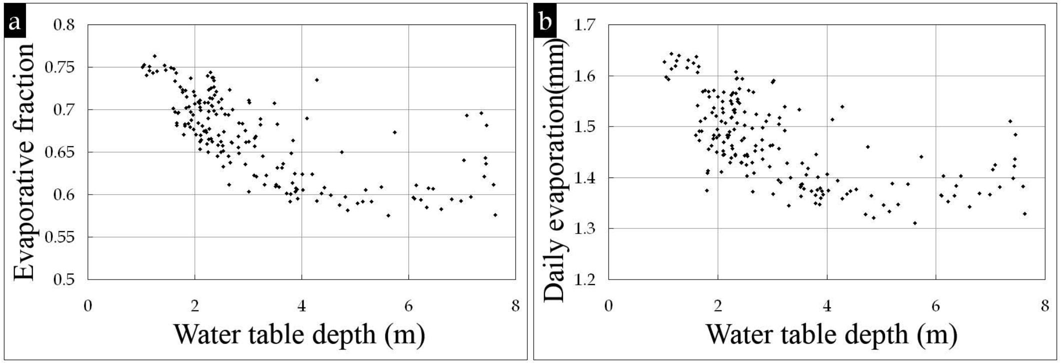


**Fig. 10.** The cross-relationships between water table depth and **(a)** the evaporative fraction and **(b)** the actual daily evaporation.





HESSD
8, 8671–8700, 2011

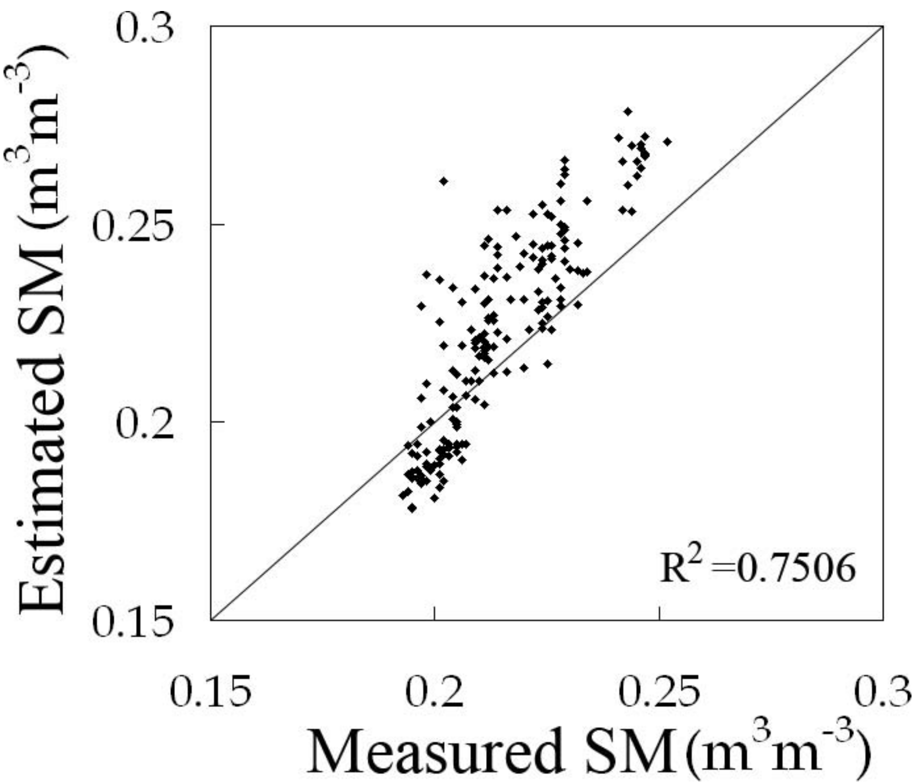


**Fig. 11.** Soil moisture of the upper 5 cm measured in field by Stevens' Hydra probe against soil moisture estimated from evaporative fraction using Eq. (11).





HESSD
8, 8671–8700, 2011



Title Page
Abstract | Introduction
Conclusions | References
Tables | Figures
◄ | ►
Back | Close
Full Screen / Esc
Printer-friendly Version
Interactive Discussion